Energy Storage Materials 27 (2020) 205–211

Contents lists available at ScienceDirect

Energy Storage Materials

journal homepage: www.elsevier.com/locate/ensm

Chemically resistant Cu–Zn/Zn composite anode for long cycling aqueous batteries

Zhao Cai , Yangtao Ou , Jindi Wang , Run Xiao , Lin Fu , Zhu Yuan , Renmin Zhan , Yongming Sun *

Wuhan National Laboratory for Optoelectronics, Huazhong University of Science and Technology, Wuhan, 430074, China

ARTICLE INFO

Keywords:
Rechargeable aqueous batteries
Zn metal anode
Chemical corrosion
Cu–Zn alloy
Electrochemical performance

ABSTRACT

Rechargeable aqueous Zn metal batteries are promising candidates for renewable energy storage. However, Zn metal is chemically active and suffers from chemical corrosion in aqueous electrolyte due to its low redox potential. It is of vital importance to reveal the corrosion mechanism, and improve the chemical stability and electrochemical reversibility of Zn metal anode for its practical application. In this work, it is revealed that a Zn metal electrode readily gets oxidized during its resting in aqueous $ZnSO_4$ electrolyte, forming zinc hydroxide sulfate and hydrogen gas, leading to the increased internal resistance and swollen problems of batteries, and eventually battery failure. To inhibit such chemical corrosion, an anti-corrosive metallic Cu is introduced to Zn metal anode to construct a uniform Cu/Zn composite with dense structure, which is electrochemically converted to Cu–Zn alloy/Zn composite during battery cycling. The as-achieved Cu–Zn/Zn electrode exhibits stable cycling for over 1500 cycles at 1 mA/cm^2 and 0.5 mAh/cm^2 with little change in overpotential (46 mV) after resting for 1 month, while the bare Zn electrode shows large voltage fluctuation and high overpotential (>400 mV) under the same condition, suggesting the importance of inhibiting the chemical corrosion of Zn metal anode for rechargeable aqueous batteries.

1. Introduction

The unprecedented development of technologies, including electric vehicles, portable electronics, and grid energy storage, calls for efficient energy storage devices with low cost, long lifespan and high safety [1–12]. Rechargeable batteries employing Zn metal anode and aqueous electrolyte are emerging as strong candidates due to their cost-effectiveness, high safety, environmental friendliness, and considerable energy density [13–20]. Particularly, Zn metal offers a number of advantages as a battery anode, including high theoretical capacity (820 mAh/g), low redox potential (−0.76 V *vs.* standard hydrogen electrode (SHE)) and high abundance [21]. However, it remains a great challenge to achieve high-performance Zn metal anode with high stability and electrochemical reversibility due to the severe problems such as Zn dendrite growth and corrosion [22–25]. To improve the electrochemical reversibility of Zn metal anode, several important strategies, including employing stable metallic Zn host/substrate [26–30], using protective surface layer [31–34], 3D structured metallic Zn [35], electrolyte engineering (e.g., "water-in-deep eutectic solvent" electrolyte [36], electrolyte additives [37], organic electrolyte [38], and molten salt electrolyte [39]), as well as construction of *in-situ* solid electrolyte interphase [40], have been proposed and exciting progresses have been achieved. However, a significant challenge, corrosion of Zn metal anode in aqueous electrolyte [41], still remains, which causes the instability of Zn metal electrode during the battery resting and cycling, and inhibits its practical application in rechargeable aqueous batteries.

Due to the chemical reactivity of Zn metal in aqueous electrolyte at room temperature, non-conducting oxides/hydroxides tend to form on the surface of the Zn metal electrode [42], which consumes active metallic Zn and electrolyte, causes gas evolution, increases the impedance of the batteries, and eventually leads to the degradation of battery performance. Till now, the full understanding of corrosion mechanism of Zn metal anode in aqueous electrolyte is still lacking [43]. Therefore, it is of vital importance to figure out the corrosion mechanism and explore strategies to inhibit the corrosion of Zn metal electrode in aqueous electrolyte during both the dwell time and electrochemical cycling of batteries.

In this work, we investigated the corrosion of Zn metal electrode in a typical mild acidic $ZnSO_4$ aqueous electrolyte, which is widely used in rechargeable aqueous Zn metal batteries because of its cost-effectiveness and good stability [44,45]. We uncovered that the corrosion of Zn metal in 3 M $ZnSO_4$ electrolyte started from the surface accessible to the

* Corresponding author.
E-mail address: yongmingsun@hust.edu.cn (Y. Sun).

https://doi.org/10.1016/j.ensm.2020.01.032
Received 3 December 2019; Received in revised form 21 January 2020; Accepted 31 January 2020
Available online 5 February 2020

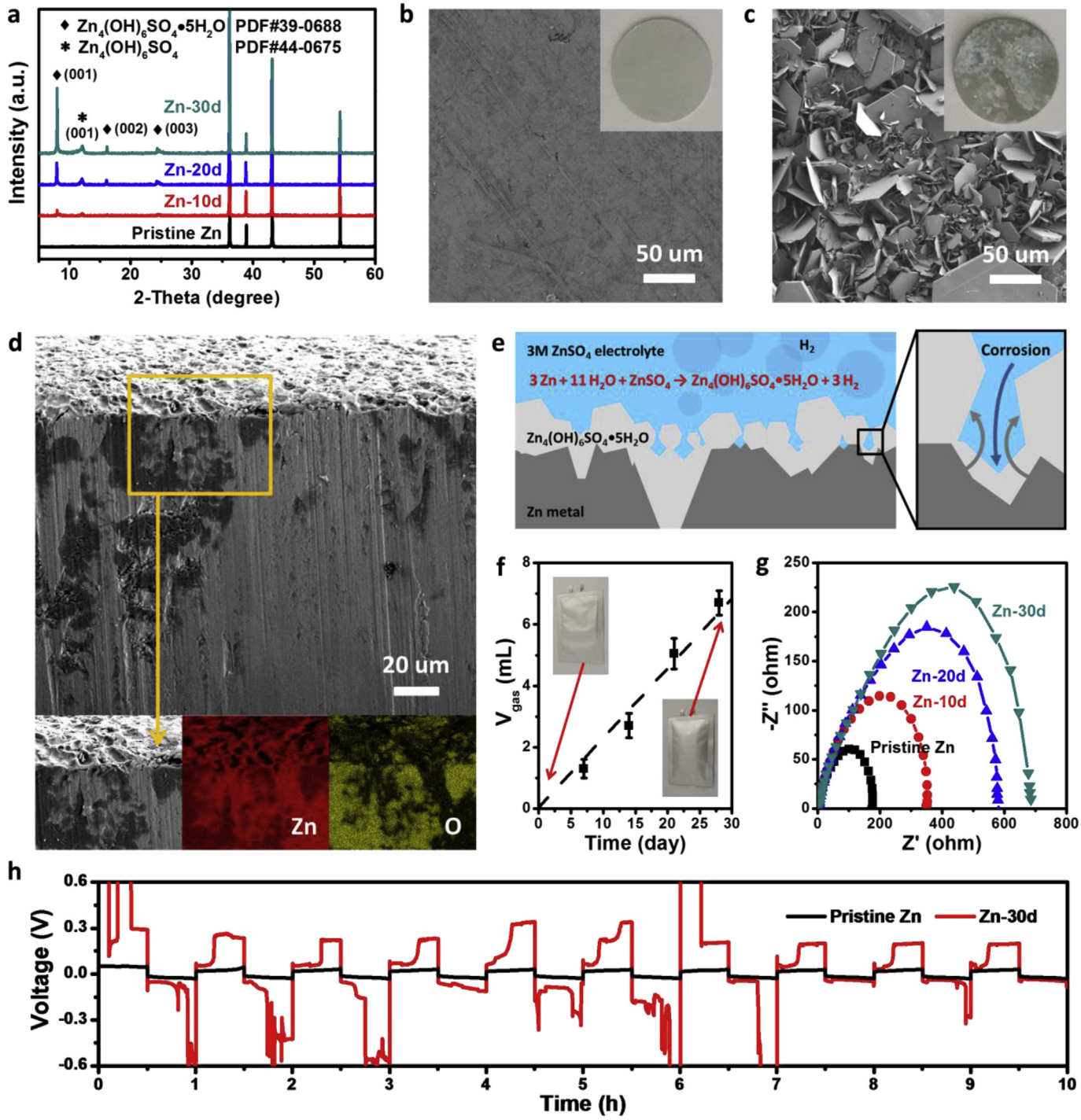

Fig. 1. Chemical corrosion of Zn metal anode in mild acidic aqueous electrolyte. (a) XRD analysis of Zn metal electrode resting in 3 M $ZnSO_4$ electrolyte for different times. Top-view SEM images of (b) pristine Zn electrode and (c) Zn-30d electrode. The insets showed the digital pictures of the corresponding electrodes. (d) Cross-section SEM and EDS elemental mapping results of the Zn-30d electrode. (e) Schematic illustration of the chemical corrosion of Zn metal electrode in 3 M $ZnSO_4$ electrolyte. (f) The gas evolution accompanied by the Zn chemical corrosion in 3 M $ZnSO_4$ electrolyte. (g) EIS results of the Zn||Zn symmetrical cells with 3 M $ZnSO_4$ electrolyte after resting for different times. (h) Voltage profiles of symmetric cells assembled using pristine Zn and Zn-30d electrode, demonstrating the corrosive nature of Zn metal anode in aqueous electrolyte.

electrolyte, where $Zn_4(OH)_6SO_4$ microsheets were first formed, accompanying with the evolution of hydrogen gas. Then, the $Zn_4(OH)_6SO_4$ intermediates were hydrated and transformed to $Zn_4(OH)_6SO_4{\cdot}5H_2O$, resulting in significant corrosion of Zn metallic electrode. It should be noted that the corrosion of Zn metal was not uniform. The deepest corrosion pit reached 132.2 μm after a dwell time of 30 days. The as-formed deactivated Zn side product, gas evolution, and consumption of electrolyte would increase electrochemical impedance of Zn metal anode and lead to battery degradation. Given that, we introduced chemically inert metallic Cu to improve the anti-corrosive property of Zn metal electrode. A simple replacement reaction was utilized to construct a uniform Cu/Zn composite with dense structure, which was electrochemically converted to Cu–Zn nanoalloy/Zn hybrid during battery cycling. As expected, such Cu–Zn/Zn electrode displayed much better

stability and electrochemical reversibility than the pristine Zn metal anode. A Cu–Zn/Zn||Cu–Zn/Zn symmetric cell showed stable electrochemical cycling of 1500 cycles at 1 mA/cm^2 with a fixed capacity of 0.5 mAh/cm^2 with little change in overpotential (46 mV) after a dwell time of 30 days, suggesting the remarkable anti-corrosion property and electrochemical reversibility of the Cu–Zn/Zn electrode. In contrast, the Zn|| Zn symmetric cell failed and could not cycle after a dwell time of 30 days. Moreover, the Cu–Zn/Zn||Cu–Zn/Zn symmetric cell exhibited stable electrochemical performance for 648 h under a measurement with a combination of electrochemically Zn stripping/plating cycling (72 cycles, 1 mA/cm^2, 0.5 mAh/cm^2) and resting (72 h), and looping.

2. Results and discussion

The chemical corrosion behavior of Zn metal electrode in 3 M $ZnSO_4$ electrolyte was first investigated using X-ray diffraction (XRD). As shown in Fig. 1a, the diffraction peaks of triclinic $Zn_4(OH)_6SO_4$ were observed for the Zn electrode after resting in 3 M $ZnSO_4$ electrolyte for 10 days (denoted as "Zn-10d"), suggesting the quick chemical corrosion of Zn metal in aqueous electrolyte. The $Zn_4(OH)_6SO_4$ was then hydrated to form triclinic $Zn_4(OH)_6SO_4{\cdot}5H_2O$, as evidenced by the XRD results for the Zn electrode after a dwell time of 20 and 30 days (denoted as "Zn-20d" and "Zn-30d", respectively). As revealed by scanning electron microscopy (SEM), the initial smooth surface of Zn metal electrode became rough and $Zn_4(OH)_6SO_4$ side product was emerged after resting in 3 M $ZnSO_4$ electrolyte for 10 days (Fig. b, S1). 30 days later, a loose layer of sheetlike $Zn_4(OH)_6SO_4{\cdot}5H_2O$ was formed on the surface of the Zn metal anode (Fig. 1c). Such corrosion of Zn metal was severe and even visible by the naked eye (insets, Fig. 1b and c). White side products were distributed on the surface of the Zn-30d electrode unevenly, suggesting the inhomogeneous chemical corrosion. The cross-section SEM image of the Zn-30 electrode showed that dense Zn metal was covered by a non-uniform porous/loose layer of side products. The thickness of this porous layer could be identified by the signal of oxygen in the corresponding energy dispersive spectroscopy (EDS) elemental images and it reached as high as 132.2 μm in a certain location (Fig. 1d, S2). These results suggested the serious chemical corrosion of Zn metal in aqueous electrolyte. During the corrosion process, the as-formed loose layer further led the permeation of electrolyte to the bulk Zn metal and caused the continuous corrosion (Fig. 1e). As a result, the surface of Zn metal anode would be never passivated and the corrosion would continue until the run out of the liquid electrolyte or active metallic Zn. We noted that the chemical corrosion of Zn metal was accompanied by the evolution of gas bubble products. The amount of gas generated due to corrosion during battery resting was studied using a Zn||Zn symmetric cell with a pouch cell configuration (Fig. 1f). With the size of 4 × 4 cm^2 for the Zn metal electrodes, ~6.7 mL of hydrogen gas was produced after a dwell time of 28 days. Accordingly, ~19.8 μL of electrolyte was consumed and 15.9 mAh of active Zn metal was oxidized/deactivated (Figs. S3 and S4). As a result, the battery performance would degrade or the battery would even fail after a dwell time. It should be noted that some of the cells exploded due to the evolution of gas (Fig. S5). We compared the electrochemical impedance and cycling behavior of a Zn||Zn symmetric cell in a coin cell configuration before and after different dwell times. As shown in Fig. 1g, the fresh Zn||Zn symmetric cell showed a charge transfer resistance (R_{ct}) of ~177 Ω. After resting for different times (10 days and 20 days), significant increase in battery impedance was observed, with R_{ct} of ~352 Ω for Zn-10d and ~580 Ω for Zn-20d, respectively. The R_{ct} of Zn||Zn symmetrical cell after a dwell time of 30 days reached ~685 Ω, which was nearly 3 times higher than the fresh one. The increased electrochemical resistance of Zn metal electrode caused severe battery performance degradation. As shown in Fig. 1h, in comparisons to the stable voltage plots and low overpotential (~48 mV) for the pristine Zn, the

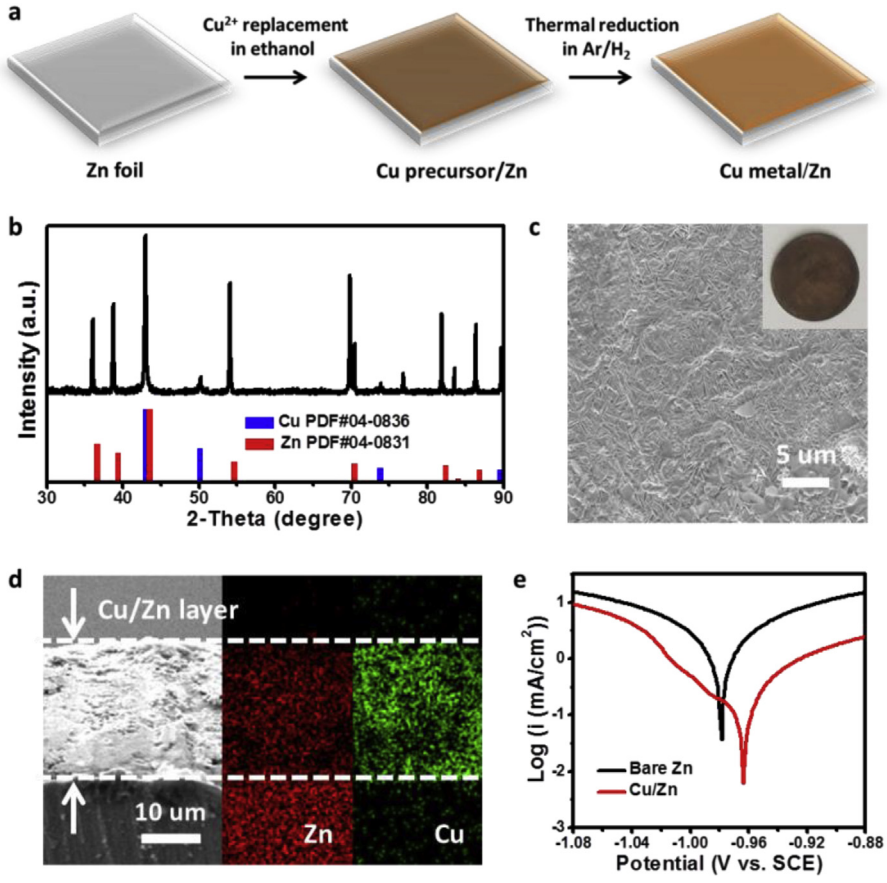

Fig. 2. Fabrication of the Cu/Zn electrode. (a) Schematic illustration of the fabrication process of the Cu/Zn electrode. (b) XRD pattern of the Cu/Zn electrode. (c) Top-view SEM image of the Cu/Zn electrode. The inset showed a digital picture of the as-prepared Cu/Zn electrode. (d) Cross-section SEM and EDS elemental mapping images of the Cu/Zn electrode. (e) Linear polarization curve of the Cu/Zn electrode in 3 M $ZnSO_4$ electrolyte, suggesting that the corrosion was suppressed for the Cu/Zn electrode in comparison to the bare Zn electrode.

Zn-30d electrode showed large fluctuation in voltage plots and high overpotential (>400 mV). These results indicated the significant influence of corrosion on the electrochemical behavior of a Zn metal electrode. Thus, close attention should be paid to the corrosion during the evaluation and application of Zn metal anode.

To inhibit the corrosion of Zn metal electrode in aqueous electrolyte, protective Cu metal was introduced and a Cu/Zn composite electrode was fabricated. Metallic Cu has good chemical stability in aqueous electrolyte due to the positive electrode potential of Cu metal (+0.34 V *vs.* SHE). Also, metallic Cu is highly conductive and can be alloyed with Zn to guide the deposition of metallic Zn [46]. A Cu/Zn composite structure on Zn foil was fabricated utilizing the galvanic reaction between metallic Zn and Cu^{2+} in ethanol, followed by an annealing process to form an integrated Cu/Zn structure (Fig. 2a). The successful fabrication of Cu/Zn composite was confirmed by the XRD result (Fig. 2b). The color turned from silver-white for the initial pure Zn metal foil to dark red for the Cu/Zn composite foil after the reaction (inset of Fig. 2c). The top-view SEM image showed the smooth surface of the as-fabricated Cu/Zn electrode (Fig. 2c). To further investigate the structure of the Cu/Zn composite, cross-section SEM image was performed, which showed a dense and integrated structure. The corresponding EDS elemental mapping indicated that the Cu/Zn composite layer was uniform over the entire observed area and the thickness of the Cu/Zn composite layer was 20.1 ± 0.9 μm (Fig. 2d). The overall Cu/Zn atomic ratio was determined to be about 1:1 (Fig. S6). Interestingly, Cu was rich on the very surface in comparison to the subjacent layer of the Cu/Zn composite (Fig. S7). With the incorporation of chemically stable Cu metal and the Cu-rich very surface layer, corrosion reaction of the Zn metal electrode was suppressed. As analyzed by linear polarization measurements in 3 M $ZnSO_4$ electrolyte (Fig. 2e), the corrosion potential of Cu/Zn electrode (−0.964 V) was higher than bare Zn electrode (−0.976 V). A more positive corrosion potential of the Cu/Zn composite electrode than the bare Zn electrode suggested the improved chemical stability. More importantly, the corrosion current of the Cu/Zn composite electrode (6.03 μA/cm^2) was only one sixth of the bare Zn electrode (37.15 μA/cm^2), indicating a much lower corrosion rate of the Cu/Zn composite electrode in aqueous electrolyte. Therefore, improved electrochemical performance of the Cu/Zn electrode can be expected due to its good anti-corrosion capability.

Cu/Zn||Cu/Zn symmetric cells were assembled using 3 M $ZnSO_4$ aqueous electrolyte. The structural stability of the Cu/Zn electrode and its electrochemical performance were investigated after a dwell time of 30 days (namely Cu/Zn-30d). The cross-section and top-view SEM images showed that the initial Cu/Zn composite structure was well maintained without change after a dwell time of 30 days (Fig. 3a, S8, 2d), while significant change in morphology and phase were observed for the bare Zn metal electrode before and after its resting in aqueous electrolyte (Fig. 1a–d). Also, no new phase (e.g., $Zn_4(OH)_6SO_4{\cdot}5H_2O$) was formed for the Cu/Zn-30d electrode, as evidenced by XRD measurement (Fig. S9). We noted that the Cu/Zn electrode produced only ~1.3 mL of

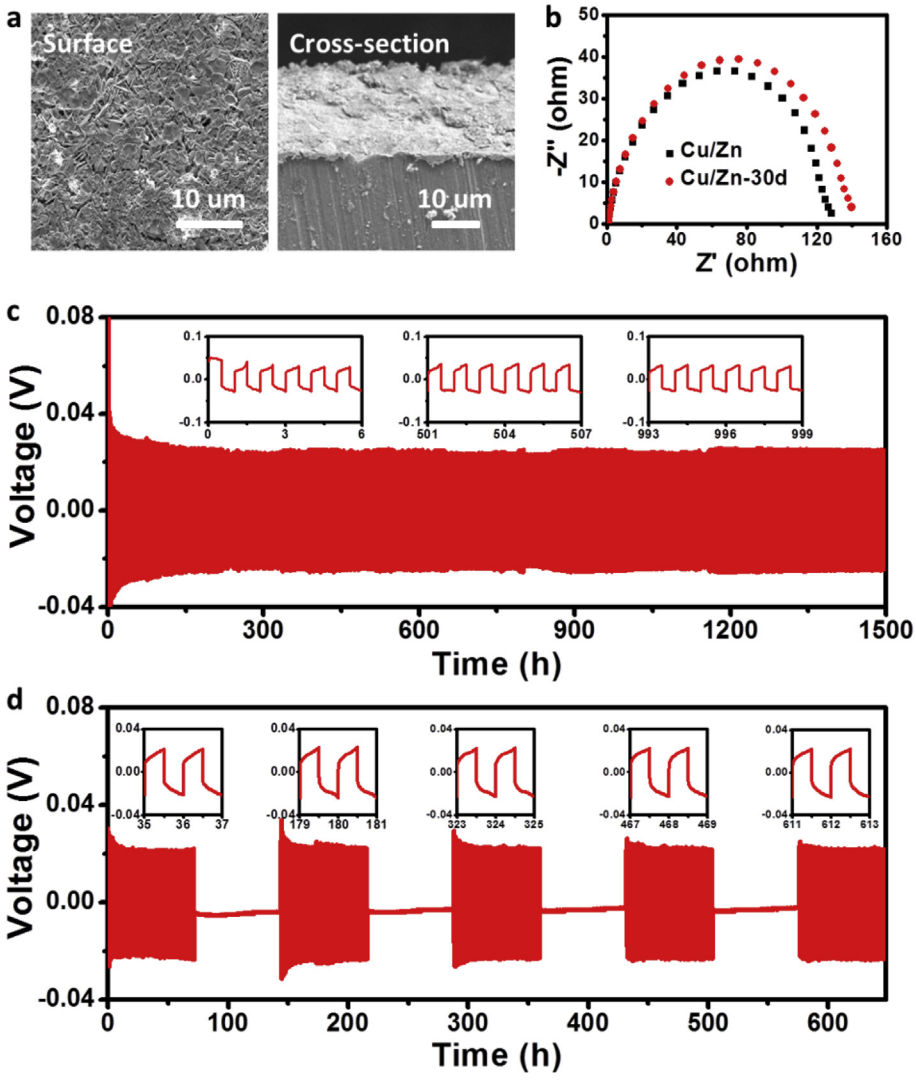

Fig. 3. Electrochemical performance of Cu/Zn electrode in aqueous electrolyte. (a) The top-view and cross-section SEM images of Cu/Zn-30d electrode. (b) EIS results of Cu/Zn and Cu/Zn-30d electrodes. (c) Voltage profiles of Cu/Zn-30d||Cu/Zn-30d symmetric cell at 1 mA/cm^2 and 0.5 mAh/cm^2, the insets showed the high-resolution voltage profiles at different times. (d) Dynamic measurement of Cu/Zn||Cu/Zn symmetric cell with a combination of Zn stripping/plating cycling (72 cycles, 1 mA/cm^2, 0.5 mAh/cm^2) and resting (72 h), and looping. The insets showed the high-resolution voltage profiles for specific working cycles. The Cu/Zn electrode exhibited stable voltage response when switching between cycling and resting conditions, suggesting the excellent unti-corrosion ability.

hydrogen gas after a dwell time of 28 days (Fig. S10), which was only 19.4% of that for bare Zn electrode under the same condition. Moreover, the Cu/Zn||Cu/Zn cell maintained its initial shape while the Zn||Zn cell exploded after a dwell time of 30 days, suggesting that the gas evolution was also significantly suppressed by using Cu/Zn electrodes (Fig. S11). Moreover, there was very little change in impedance for the fresh Cu/Zn electrode and Cu/Zn-30d electrode (Fig. 3b). These results implied the much improved stability of the Cu/Zn electrode in aqueous electrolyte. Thus, improved electrochemical performance could be expected for the Cu/Zn-30d electrode. As shown in Fig. 3c, the Cu/Zn-30d electrode displayed extremely stable electrochemical stripping/plating behavior with an overptential of ~46 mV for 1500 cycles in sharp contrast to the bare Zn metal anode (Zn-30d), which failed to cycle after a dwell time of 30 days (Fig. 1h). Additionally, the fresh Cu/Zn electrode exhibited much better cycling stability than the fresh bare Zn electrode (stable cycling over 500 cycles with overpotential of ~44 mV for Cu/Zn *vs.* gradually increased overpotential from ~48 to 120 mV after 60 cycles for bare Zn), indicating the important role of introduced anti-corrosive Cu components in suppressing the corrosion during cycling and improving the electrochemical performance (Fig. S12).

To further demonstrate the advancement of the Cu/Zn electrode in suppressing corrosion and improving the electrochemical performance, Coulombic efficiency (CE) of the bare Zn and Cu/Zn electrodes were compared by electrochemical cycling of cells using thin bare Zn and Cu/Zn working electrodes on Ti foil. As shown in Fig. S13, the average CE of the Cu/Zn electrode was determined to be 91.8%, higher than that of the bare Zn (81.3%) for 100 cycles at 5 mA/cm^2 and 0.5 mAh/cm^2, demonstrating the enhanced electrochemical reversibility. Furthermore, dynamic measurement was performed with a combination of electrochemical stripping/plating cycling (72 cycles, 1 mA/cm^2, 0.5 mAh/cm^2) and resting (72 h), and looping (Fig. 3d). With alternative cycling and resting measurement, the Cu/Zn||Cu/Zn symmetric cell exhibited robust electrochemical performance. Recovering after each period of resting, the Cu/Zn electrode exhibited stable cycling with a low average overpotential of ~48 mV. Stable performance remained even after 648 h' testing. We further prepared MnO_2 on carbon cloth (MnO_2@CC) electrode and used it to pair with Cu/Zn electrode to assemble full cells and evaluate the practicability of the Cu/Zn anode. Fig. S14 showed that the bare Zn||MnO_2 full cell maintained only 27.6% of its initial capacity after 300 cycles at a rate of 10 *C* (1*C* = 308 mAh/g, based on MnO_2). Meanwhile, the Cu/Zn||MnO_2 full cell exhibited excellent cycling stability, which delivered 94.2% of its initial capacity after 500 cycles. Such robust electrochemical performance supports the practical application of Cu/Zn electrode in rechargeable aqueous batteries.

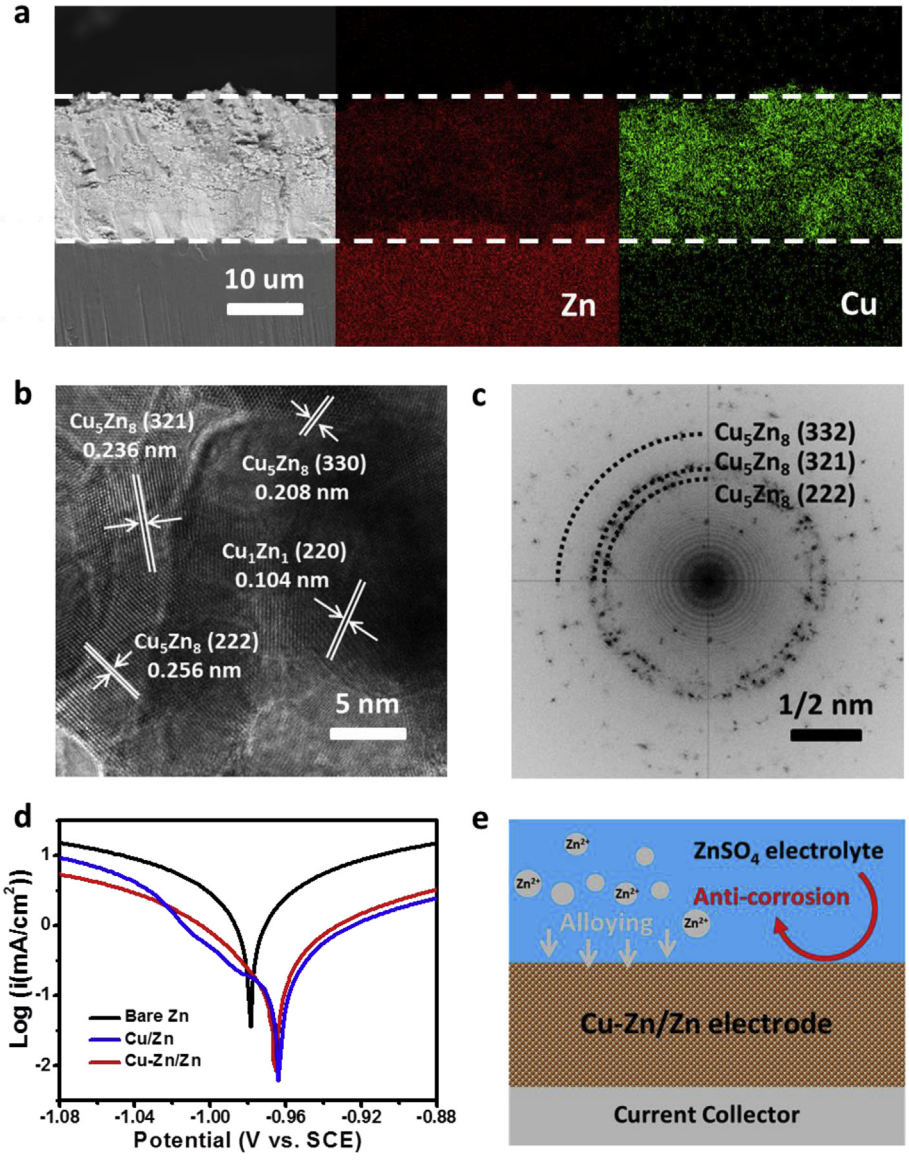

Fig. 4. Structure of Cu/Zn electrode after cycling. (a) Cross-section SEM and EDS elemental mapping images of the Cu/Zn electrode after 100 stripping/plating cycles. (b) HRTEM image and (c) SAED pattern of the Cu/Zn electrode after 100 stripping/plating cycles. These results indicated the formation of Cu–Zn alloy on the surface of the electrode during cycling. (d) Linear polarization curve of Cu/Zn and Cu–Zn/Zn electrode in 3 M $ZnSO_4$ electrolyte. (e) Schematic illustration of the function of the Cu–Zn alloy on Cu–Zn/Zn electrode.

The structural stability of cycled Cu/Zn electrode was investigated by SEM and transmission microscope (TEM). Fig. 4a showed the cross-sectional SEM image of the Cu/Zn electrode after 100 stripping/plating cycles. A dense structure with thickness of 19.6 ± 1.5 μm was observed for the Cu/Zn electrode after cycling, which was almost the same as the fresh Cu/Zn electrode before cycling (Fig. 2d). Moreover, the surface of the cycled Cu/Zn electrode remained smooth (Fig. S15). In contrast, porous surface layer and sheetlike side product were formed for the cycled bare Zn electrode (Fig. S16). These results demonstrated the good stability of Cu/Zn electrode during electrochemical cycling. Detail structural information of the Cu/Zn electrode after cycling was further analyzed using TEM. The cycled Cu/Zn composite sample was scraped from the surface of the cycled Cu/Zn electrode, and a dense structure consisting of interconnected nanoparticles was observed (Fig. S17). The EDS elemental mapping in the TEM indicated the heterogeneous distribution of Cu and Zn elements in each measured nanoparticle (Fig. S18). High resolution TEM (HRTEM) image showed the clear lattice fringes of Cu–Zn alloy (Cu_5Zn_8 and Cu_1Zn_1), suggesting the formation of Cu–Zn alloy during the electrochemical cycling (Fig. 4b). Moreover, the result of selected area electron diffraction (SAED) pattern indicated that the as-formed Cu–Zn alloy was mainly Cu_5Zn_8 (Fig. 4c). Thus, Cu–Zn alloy was *in-situ* formed during electrochemical cycling on the surface of the Cu/Zn electrode. We also tested the anti-corrosion capability of the as-formed Cu–Zn/Zn electrode after cycling. As shown in Fig. 4d, both the corrosion potential and current density of the Cu–Zn/Zn electrode (−0.966 V, 7.94 μA/cm^2) were quite similar to that of the fresh Cu/Zn electrode (−0.964 V, 6.03 μA/cm^2). These finding demonstrated the excellent anti-corrosion capability of the cycled Cu–Zn/Zn electrode (Fig. 4e). Therefore, the corrosion reaction was significantly suppressed for the Cu/Zn electrode during its whole lifecycle (dwell time and cycling) and the electrochemical performance of the electrode was greatly improved (Figs. 2 and 3).

3. Conclusion

In summary, the chemical corrosion of Zn metal electrode in 3 M $ZnSO_4$ aqueous electrolyte has been investigated. Zn metal electrode tends to be oxidized inhomogeneously in aqueous $ZnSO_4$ electrolyte at room temperature, accompanied with in the formation of loose surficial layer of zinc hydroxide sulfate and gas evolution. The chemical corrosion of Zn metal anode leads to the consumption of electrolyte and active metallic Zn, increase in electrode impedance, and finally failure of batteries. To suppress the chemical corrosion of Zn metal anode, a uniform Cu/Zn composite with dense structure was constructed. The as-fabricated Cu/Zn anode showed much improved stability in comparison to the bare Zn electrode due to the good chemical stability and more positive electrode potential of Cu, and exhibited a much reduced corrosion rate (−0.964 V, 6.03 μA/cm^2 for Cu/Zn *vs.* −0.976 V, 37.15 μA/cm^2 for bare Zn) in aqueous electrolyte. During electrochemical cycling, the Cu/Zn electrode was converted to Cu–Zn alloy/Zn electrode, which maintained good chemical and electrochemical stability. Significantly, the Cu–Zn/Zn electrode showed stable electrochemical stripping/plating cycling for over 1500 cycles with a low overpotential of ~46 mV at 1 mA/cm^2 and 0.5 mAh/cm^2 after a dwell time of 1 month. This work provides fundamental understanding of the corrosion of Zn metal electrode in aqueous batteries, shows the important influence of corrosion on electrochemical performance of Zn metal electrode, and sheds light on the rational design of anti-corrosion Zn anode for stable and deeply rechargeable aqueous batteries.

4. Experimental section

4.1. Preparation of Cu/Zn electrode

Zn metal foil was firstly cut into disks with diameter of 12 mm and washed with diluted hydrochloric acid for 3 min to remove the surficial oxide layer. After washing with deionized water and ethanol, the cleaned Zn foil was immersed in a 0.1 M $CuCl_2$ solution in ethanol for 10 min. After rinsing with deionized water for several times, the foil was annealed under an Ar/H_2 atmosphere (5vol % H_2) at 300 °C for 2 h.

4.2. Materials characterization

XRD measurements were carried out on an Empyrean X-ray diffractometer with Cu Kα radiation (40 kV, 30 mA, λ = 1.5418 Å), recorded with 2θ ranging from 10° to 90°. TEM was performed with FEI Tecnai G^2 F30 instrument. SEM studies were performed on a Gemini SEM 300 field-emission SEM instrument.

4.3. Electrochemical measurements

To evaluate the electrochemical stripping/plating behavior and cycling stability of the Zn and Cu/Zn electrodes, symmetric cells were assembled using glass fiber as the separator and 3 M $ZnSO_4$ as the electrolyte in standard CR2032 coin-type cells. The cells were tested at a current density of 1 mA/cm^2 with a fixed capacity of 0.5 mAh/cm^2 on a NEWARE battery tester. A Biologic VMP3 electrochemical workstation was employed to study the electrochemical property of Zn metal electrode with a three-electrode system. A saturated calomel electrode and a graphite rod were used as the reference and the counter electrode, respectively. The polarization data were collected using linear sweep voltammetry at a scan rate of 1 mV/s to minimize capacitive current. AC impedance measurements were carried out at open-circuit voltage from 0.1 to 10^5 Hz with an AC voltage of 5 mV.

4.4. Determination of the volume of gas generated during Zn chemical corrosion

Zn||Zn symmetric cell in a pouch configuration with an electrode size of 4 × 4 cm^2 and using $ZnSO_4$ aqueous electrolyte was fabricated and the volume of hydrogen gas produced due to chemical corrosion during resting was measured. After resting for different times (e.g. 7, 14, 21, 28 days), the generated gas was extracted and recorded by a disposable syringe measured with a minimum precision of 0.05 mL.

4.5. Determination of Coulombic efficiency

The bare Zn/Ti electrode was prepared by an electrodeposition method using a three-electrode system, where a Ti foil was used as working electrode and a Zn foil was used as both the counter and reference electrode. Zn metal was electrodeposited on Ti foil under a constant current density of 20 mA/cm^2 in 1 M $ZnSO_4$ electrolyte to produce a Zn/Ti electrode. Cu/Zn/Ti electrode was fabricated by immersing Zn/Ti electrode in a 0.1 M $CuCl_2$ solution in ethanol for 10 min and then annealing under an Ar/H_2 atmosphere (5vol % H_2) at 300 °C for 2 h. To evaluate the Coulombic efficiency of the Cu/Zn/Ti and Zn/Ti electrodes, active areal capacities (Qs) for the fresh electrodes were first measured by complete electrochemical stripping test in Cu/Zn/Ti||Zn and Zn/Ti||Zn cells using bare Zn metal foil as the counter electrode with cut-off voltage of 1 V. respectively. Also other fresh Cu/Zn/Ti||Zn and Zn/Ti||Zn cells with the same working electrodes were cycled at 5 mA/cm^2 and 0.5 mAh/cm^2 (Q_T) and the areal capacities (Qc) of Cu/Zn/Ti and Zn/Ti electrodes after 100 cycles were obtained after complete electrochemical stripping of metallic Zn of these working electrodes. The average CE of Cu/Zn/Ti and Cu/Ti electrodes were then calculated [$CE = 1-(Q_S-Q_C)/(100^* Q_T)$].

4.6. Zn||MnO_2 full cells assembly

The MnO_2@CC electrode was prepared with a two-electrode system in 3 M $ZnSO_4$ +0.3 M $MnSO_4$ aqueous electrolyte, where a CC and a Zn metal foil were used as the working and the counter electrode,

respectively. A constant voltage of 1.8 V was applied for 8 h using an electrochemical workstation (BioLogic VSP, Claix) to deposit MnO_2 on CC. The mass loading of MnO_2 on CC was ~1.0 mg/cm^2. Zn||MnO_2 full cells were assembled in standard CR2032 coin-type cells using Zn metal foil as the anode, 3 M $ZnSO_4$ +0.1 M $MnSO_4$ aqueous solution as electrolyte, and the MnO_2@CC as the cathode.

Declaration of competing interest

The authors declare that they have no known competing financial interests or personal relationships that could have appeared to influence the work reported in this paper.

CRediT authorship contribution statement

Zhao Cai: Investigation, Data curation, Writing - original draft. **Yangtao Ou:** Investigation, Data curation. **Jindi Wang:** Investigation, Methodology. **Run Xiao:** Investigation. **Lin Fu:** Investigation, Data curation. **Zhu Yuan:** Investigation. **Renmin Zhan:** Investigation. **Yongming Sun:** Supervision, Conceptualization, Methodology, Writing - review & editing.

Acknowledgements

Y. S. acknowledges the financial support by the Innovation Fund of Wuhan National Laboratory for Optoelectronics of Huazhong University of Science and Technology. Z. C. thanks the China Postdoctoral Science Foundation (No. 2018M640694). The authors would like to thank the Analytical and Testing Center of Huazhong University of Science and Technology as well as the Center for Nanoscale Characterization & Devices of Wuhan National Laboratory for Optoelectronics for providing the facilities to conduct the characterization.

Appendix A. Supplementary data

Supplementary data to this article can be found online at https://doi.org/10.1016/j.ensm.2020.01.032.

References

[1] F. Wang, O. Borodin, T. Gao, X. Fan, W. Sun, F. Han, A. Faraone, J.A. Dura, K. Xu, C. Wang, Nat. Mater. 17 (2018) 543–549.
[2] J. Huang, Z. Wang, M. Hou, X. Dong, Y. Liu, Y. Wang, Y. Xia, Nat. Commun. 9 (2018) 2906.
[3] H. Pan, Y. Shao, P. Yan, Y. Cheng, K.S. Han, Z. Nie, C. Wang, J. Yang, X. Li, P. Bhattacharya, K.T. Mueller, J. Liu, Nat. Energy 1 (2016) 16039.
[4] N. Zhang, F. Cheng, J. Liu, L. Wang, X. Long, X. Liu, F. Li, J. Chen, Nat. Commun. 8 (2017) 405.
[5] P. Cai, G. Wang, K. Chen, Z. Wen, J. Power Sources 428 (2019) 37–43.
[6] Z. Zhao, X. Fan, J. Ding, W. Hu, C. Zhong, J. Lu, ACS Energy Lett. 4 (2019) 2259–2270.
[7] L. Chen, Z. Yang, Y. Huang, Nanoscale 11 (2017) 13032–13039.
[8] Y. Zhang, Q. Su, W. Xu, G. Cao, Y. Wang, A. Pan, S. Liang, Adv. Sci. 6 (2019), 1900162.
[9] Q. Wang, Z. Zhang, M. Wang, F. Liu, L. Jiang, B. Hong, J. Li, Y. Lai, Nanoscale 10 (2018) 15819–15825.
[10] Y. Cai, G. Fang, J. Zhou, S. Liu, Z. Luo, A. Pan, G. Cao, S. Liang, Nano Res. 11 (2018) 449–463.
[11] J. Tang, Q. Yin, Q. Wang, Q. Li, H. Wang, Z. Xu, H. Yao, J. Yang, X. Zhou, J.-K. Kim, L. Zhou, Nanoscale 11 (2019) 10984–10991.
[12] M. Xu, L. Fei, W. Zhang, T. Li, W. Lu, N. Zhang, Y. Lai, Z. Zhang, J. Fang, K. Zhang, J. Li, H. Huang, Nano Lett. 17 (2017) 1670–1677.
[13] G.G. Yadav, D.E. Turney, J. Huang, X. Wei, S. Banerjee, ACS Energy Lett. 4 (2019) 2144–2146.
[14] T. Xiong, Z. Gen Yu, H. Wu, Y. Du, Q. Xie, J. Chen, Y.W. Zhang, S.J. Pennycook, W.S.V. Lee, J. Xue, Adv. Energy Mater. 9 (2019) 1803815.
[15] D. Chao, W. Zhou, C. Ye, Q. Zhang, Y. Chen, L. Gu, K. Davey, S.Z. Qiao, Angew. Chem. Int. Ed. 58 (2019) 7823–7828.
[16] F. Wang, E. Hu, W. Sun, T. Gao, X. Ji, X. Fan, F. Han, X.Q. Yang, K. Xu, C. Wang, Energy Environ. Sci. 11 (2018) 3168–3175.
[17] K.W. Nam, H. Kim, J.H. Choi, J.W. Choi, Energy Environ. Sci. 12 (2019) 1999–2009.
[18] Q. Han, X. Chia, Y. Liua, L. Wang, Y. Du, Y. Rend, Y. Liu, J. Mater. Chem. 7 (2019) 22287–22295.
[19] D. Yuan, W.M. Jr, L. Zhang, J.J. Chan, S. Meng, Y. Chen, M. Srinivasan, ChemSusChem 12 (2019) 4889–4900.
[20] W. Sun, F. Wang, S. Hou, C. Yang, X. Fan, Z. Ma, T. Gao, F. Han, R. Hu, M. Zhu, C. Wang, J. Am. Chem. Soc. 139 (2017) 9775–9778.
[21] J. Huang, Z. Guo, Y. Ma, D. Bin, Y. Wang, Y. Xia, Small Methods 3 (2018), 1800272.
[22] M. Liu, L. Yang, H. Liu, A. Amine, Q. Zhao, Y. Song, J. Yang, K. Wang, F. Pan, ACS Appl. Mater. Interfaces 11 (2019) 32046–32051.
[23] B. Tang, L. Shan, S. Liang, J. Zhou, Energy Environ. Sci. 12 (2019) 3288–3304.
[24] V. Yufit, F. Tariq, D.S. Eastwood, M. Biton, B. Wu, P.D. Lee, N.P. Brandon, Joule 3 (2019) 485–502.
[25] W. Lu, C. Xie, H. Zhang, X. Li, ChemSusChem 11 (2018) 3996–4006.
[26] Z. Wang, J. Huang, Z. Guo, X. Dong, Y. Liu, Y. Wang, Y. Xia, Joule 3 (2019) 1289–1300.
[27] Z. Kang, C. Wu, L. Dong, W. Liu, J. Mou, J. Zhang, Z. Chang, B. Jiang, G. Wang, F. Kang, C. Xu, ACS Sustain. Chem. Eng. 7 (2019) 3364–3371.
[28] Y. Zeng, X. Zhang, R. Qin, X. Liu, P. Fang, D. Zheng, Y. Tong, X. Lu, Adv. Mater. 31 (2019), 1903675.
[29] A. Naveed, H. Yang, J. Yang, Y. Nuli, J. Wang, Angew. Chem. Int. Ed. 131 (2019) 2786–2790.
[30] C. Zhang, J. Holoubek, X. Wu, A. Daniyar, L. Zhu, C. Chen, D.P. Leonard, I.A. Rodriguez-Perez, J.X. Jiang, C. Fang, X. Ji, Chem. Commun. 54 (2018) 14097–14099.
[31] Z. Zhao, J. Zhao, Z. Hu, J. Li, J. Li, Y. Zhang, C. Wang, G. Cui, Energy Environ. Sci. 12 (2019) 1938–1949.
[32] L. Kang, M. Cui, F. Jiang, Y. Gao, H. Luo, J. Liu, W. Liang, C. Zhi, Adv. Energy Mater. 8 (2018), 1801090.
[33] K. Zhao, C. Wang, Y. Yu, M. Yan, Q. Wei, P. He, Y. Dong, Z. Zhang, X. Wang, L. Mai, Adv. Mater. Interfaces 5 (2018), 1800848.
[34] Y. Wu, Y. Zhang, Y. Ma, J.D. Howe, H. Yang, P. Chen, S. Aluri, N. Liu, Adv. Energy Mater. 8 (2018), 1802470.
[35] J.F. Parker, C.N. Chervin, I.R. Pala, M. Machler, M.F. Burz, J.W. Long, D.R. Rolison, Science 356 (2017) 415–418.
[36] J. Zhao, J. Zhang, W. Yang, B. Chen, Z. Zhao, H. Qiu, S. Dong, X. Zhou, G. Cui, L. Chen, Nano Energy 57 (2019) 625–634.
[37] W. Xua, K. Zhao, W. Huo, Y. Wang, G. Yao, X. Gu, H. Cheng, L. Mai, C. Hu, X. Wang, Nano Energy 62 (2019) 275–281.
[38] A. Naveed, H. Yang, Y. Shao, J. Yang, N. Yanna, J. Liu, S. Shi, L. Zhang, A. Ye, B. He, J. Wang, Adv. Mater. 31 (2019), 1900668.
[39] J. Zhang, J. Zhao, H. Du, Z. Zhang, S. Wang, G. Cui, Electrochim. Acta 280 (2018) 108–113.
[40] H. Qiu, X. Du, J. Zhao, Y. Wang, J. Ju, Z. Chen, Z. Hu, D. Yan, X. Zhou, G. Cui, Nat. Commun. 10 (2019) 5374.
[41] T.K.A. Hoang, T.N.L. Doan, K.E.K. Sun, P. Chen, RSC Adv. 5 (2015) 41677–41691.
[42] T.H. Wu, Y. Zhang, Z.D. Althouse, N. Liu, Mater. Today Nano 6 (2019), 100032.
[43] X. Zeng, J. Hao, Z. Wang, J. Mao, Z. Guo, Energy Storage Mater. 20 (2019) 410–437.
[44] M. Song, H. Tan, D. Chao, H.J. Fan, Adv. Funct. Mater. 28 (2018), 1802564.
[45] H. Li, L. Ma, C. Han, Z. Wang, Z. Liu, Z. Tang, C. Zhi, Nano Energy 62 (2019) 550–587.
[46] Q. Zhang, J. Luan, L. Fu, S. Wu, Y. Tang, X. Ji, H. Wang, Angew. Chem. Int. Ed. 131 (2019) 15988–15994.